Atmospheric circulation compounds anthropogenic warming and impacts of climate extremes in Europe

Davide Faranda, Gabriele Messori, Aglaé Jézéquel, Mathieu Vrac, Pascal Yiou

Atmospheric circulation compounds anthropogenic warming and extreme climate impacts in Europe

Davide Faranda[1,2,3,*], **Gabriele Messori**[4,5], **Aglae Jezequel**[3,6], **Mathieu Vrac**[1], **and Pascal Yiou**[1]

[1]Laboratoire des Sciences du Climat et de l'Environnement, CEA Saclay l'Orme des Merisiers, UMR 8212 CEA-CNRS-UVSQ, Université Paris-Saclay & IPSL, 91191, Gif-sur-Yvette, France
[2]London Mathematical Laboratory, 8 Margravine Gardens, London, W6 8RH, UK
[3]LMD/IPSL, Ecole Normale Superieure, PSL research University, 75005, Paris, France
[4]Department of Earth Sciences, Uppsala University, and Centre of Natural Hazards and Disaster Science (CNDS), Uppsala, 752 36, Sweden
[5]Department of Meteorology and Bolin Centre for Climate Research, Stockholm University, 106 91, Stockholm, Sweden
[6]Ecole des Ponts, Marne-la-Vallée, France
[*]davide.faranda@lsce.ipsl.fr

ABSTRACT

Diagnosing dynamical changes in the climate system, such as those in atmospheric circulation patterns, remains challenging. Here, we study 1950–2021 trends in the frequency of occurrence of atmospheric circulation patterns over the North Atlantic. Roughly 7% of atmospheric circulation patterns display significant occurrence trends, yet they have major impacts on surface climate. Increasingly frequent patterns drive heatwaves across Europe, and enhanced wintertime storminess in the northern part of the continent. Over 91% of recent heatwave-related deaths and 33% of high-impact windstorms in Europe were concurrent with increasingly frequent atmospheric circulation patterns. Atmospheric patterns which are becoming rarer correspond instead to wet, cool summer conditions over northern Europe and wet winter conditions over continental Europe. The combined effect of these circulation changes is that of a strong, dynamically-driven year-round warming over most of the continent and large regional and seasonal changes in precipitation and surface wind.

Main

Extreme weather events exact a heavy and steadily increasing socio-economic toll on Europe[1], eliciting both scientific and media interest in the atmospheric circulation patterns favouring the occurrence of heatwaves[2], cold spells[3], heavy precipitation[4] and windstorms[5]. Such circulation patterns may be understood as spatial patterns in a given atmospheric variable which repeatedly occur in conjunction with specific classes of extreme events. The question of whether, how and why these circulation patterns have been changing under anthropogenic forcing, including the role of Arctic Amplification, has been the source of a lively discussion[6–10].

Of particular interest is whether atmospheric circulation patterns favouring specific extreme events have become more persistent. There are several arguments supporting an increasingly persistent summer atmospheric circulation[11–13], which is highly relevant for the study of heatwaves[14,15]. Nonetheless,[10] did not find a systematic slowdown of planetary waves over the Northern Hemisphere summers in the historical period. The picture for the winter season is equally debated, with some studies finding recent increases in the sinuosity of the midlatitude flow[6] and others not finding any trends in planetary wave phase speeds[10] or arguing for a decrease in high-amplitude waves and blocking — both regarded as persistent atmospheric patterns associated with surface extremes[16]. A complementary line of work has analysed the frequency of occurrence of specific atmospheric circulation patterns associated with extreme events[17–21]. Heatwaves have again been a focus, on account of their intimate link with the large-scale atmospheric circulation and rapidly increasing frequency and duration[22]. For example,[17] found that well over half of the total trend in hot extremes over Europe may be linked to the increased occurrence of anticyclonic circulation patterns over the eastern part of the continent. Similarly,[20] argues that circulation patterns like the ones associated with the 2003 European heatwave may become increasingly frequent. Along a similar line,[21] identified observed changes in hemispheric-scale, wave-like atmospheric circulation patterns that increase the risk of concurrent heatwaves across eastern North America, eastern and northern Europe and other downstream regions in Eurasia. Other extremes, including drought[23] and heavy precipitation[24] have also been studied. The two perspectives of persistence and frequency of occurrence are intimately

related, since recurrence in a specific pattern likely translates to persistent weather and vice-versa[15].

Previous efforts in the detection of atmospheric circulation shifts have often focused on the average behaviour[6,10,12], or on a specific set of extreme events or circulation patterns[14,17,20,21,25]. Here, we consider in turn each daily atmospheric circulation pattern in 72 years of sea-level pressure reanalysis data[26], namely all daily sea-level pressure latitude-longitude maps in the geographical region and time period we analyse. The same analysis is repeated using 500 hPa geopotential height data (See Extended Data). Our approach is thus distinct from the above-cited studies. We then select those days in the winter (December–February) and summer (June–August) seasons displaying significant trends in the occurrence of their analogues (hereafter referred to simply as "occurrence trends" see Methods). The vast majority (92.7%) of circulation patterns show no significant occurrence trend in the selected/historical period; 5.1 % show increasing trends and 2.2 % show decreasing trends. Notwithstanding their rarity, the circulation patterns with significant occurrence trends have major implications for surface climate. To isolate the effect of circulation changes we also consider daily reanalysis data for 10 meter horizontal winds, 2 meter temperatures, and precipitation rates over the period 1950–2021. All the data shown in the composites are detrended and deseasonalized (see Methods).

During both the boreal summer and winter seasons, the atmospheric circulation patterns with positive occurrence trends show highly coherent surface climate anomalies over Europe. Specifically, patterns occurring more frequently in winter (Fig. 1a) show a north-south cyclonic-anticyclonic dipole. This is associated with anomalously windy, warm and wet conditions in Northern and Eastern Europe and moderately warm, dry conditions in Southern Europe (Fig. 1c, e, g). Wintertime patterns with a negative occurrence trend (Fig. 1b) have a cyclonic structure in the central North Atlantic and an anticyclone to the Northeast, leading to anomalously windy, cool and dry conditions over Northern Europe and windy, wet and moderately warm conditions over Central and Southern Europe (Fig. 1d, f, h). The average wintertime temperature and precipitation associated with patterns displaying either decreasing or increasing occurrence trends show no additional significant temporal trends over Europe (Fig. 1i, j; see mask in Extended Fig.S1).

In summer, the atmospheric circulation patterns with positive occurrence trends are associated with a extended anticyclonic anomaly over the Labrador Sea and Greenland and a cyclonic anomaly to the East of the British Isles (Fig. 2a). Such circulation patterns drive anomalously calm and dry conditions over much of the continent and anomalously warm conditions over Western Europe (Fig. fig:summerc, e, g). Circulation patterns with decreasing occurrence trends show a ridge of high pressure anomalies over the Atlantic and a large cyclonic structure centred over Northern Europe. These are associated with anomalously calm conditions over most of Europe and cool and wet conditions over Northern Europe (Fig. 2d, f, h). Again, no additional significant trends appear in summertime European precipitation or temperature associated with any of the above patterns (Figs. 2i, j).

We underline that these results are obtained for detrended and deseasonalised datasets, meaning that the observed signals are chiefly related to the atmospheric circulation. Analyses conducted on NCEP/NCAR reanalysis data (Extended Data Figs. S2,S3) and E-OBS gridded observational data (Extended Data Figs. S4,S5) provide similar conclusions. Extended Data Figs. S6–S9 further show that the atmospheric circulation patterns with positive or negative occurrence trends are generally similar at the beginning and end of the analysis period. In other words, the atmospheric circulation patterns identified as having significant occurrence trends stay roughly constant over time. The one exception are wintertime patterns with a decreasing occurrence trend (Extended Data Figs. S6a, S7a). We ascribe this difference to the very small sample sizes for these patterns, due to the fact that we consider subsets of our full analysis period in these composites.

We repeat the same analysis for the detrended 500 hPa geopotential height data (Extended Data Figs. S10, S11), to verify whether our results depend on the choice of observable for the atmospheric circulation[20]. There is a strong resemblance of the spatial anomaly composites for atmospheric circulation patterns with increasing frequency of occurrence in sea-level pressure and 500 hPa geopotential height, as well as the associated impacts on temperature, winds and precipitation (cf. Figs 2a, c, e, g, 1a, c, e, g and Extended Data Figs. S10a, c, e, g, and S11a, c, e, g). Patterns with decreasing frequency of occurrence show larger differences in both seasons (cf. Figs 2b, d, f, h, 1b, d, f, h and Extended Data Figs. S10b, d, f, h and S11b, d, f, h). This may be partly attributable to the smaller sample size for patterns with decreasing occurrence trends compared to patterns with increasing occurrence trends (approximately 43% of the sample size, computed jointly over winter and summer). It further suggests that our results for these sets of days should be interpreted with care. We conclude that the qualitative large-scale circulation patterns for days showing increasing occurrence trends and the associated surface anomalies are robust to the choice of the observable, while some notable differences emerge for days with decreasing occurrence trends.

The surface climate anomalies associated with increasingly or decreasingly frequent circulation patterns can be directly related to the occurrence of high-impact summertime heatwaves and wintertime stormy weather in Europe. We draw high-impact heatwaves and the associated excess deaths from the EM-DAT disaster database[27] (see Methods). We identify 228 heatwave days over the analysis period. 9.7% of these days correspond to atmospheric circulation patterns increasing in occurrence (versus a climatological summertime occurrence of these patterns of 4.5% and a 97.5th percentile from random sampling of 7.0%), while none correspond to decreasing occurrence trends. As a term of comparison, only 3.1% of 480

cold spell days match atmospheric circulation patterns increasing in occurrence, in line with climatology. The 228 heatwave days occur during 10 major heatwave episodes, associated with 83,462 deaths. None of the selected heatwaves include days with negative occurrence trends, while 4 of the heatwaves include an above-average fraction of days with positive occurrence trends (see Methods). The latter heatwaves are responsible for 91.4% of the total heatwave-related excess deaths[28] (Fig. 3a). Excluding the summer 2003 heatwave, which is associated with days with positive occurrence trends and alone accounts for the bulk of the total heat-related deaths in Europe in the period considered, we still find that heatwaves associated with circulation patterns with positive occurrence trends are responsible for 43.2% of total excess deaths. Although this heuristic argument is based on a limited sample of events, it nonetheless serves to illustrate the potential societal impact that circulation patterns with increasing occurrence trends may have, and motivates a future, more systematic impact-based analysis.

We conduct a similar analysis for 90 European windstorms which resulted in a high number of casualties and/or large insured losses, extending the storm database from[29] (see Methods and Extended data Fig. S12). Over a total of 438 storm days, we find that 66 (15%) are associated with circulation patterns with increasing occurrence trends and only 4 (0.9%) with patterns with decreasing trends. We find that 30 windstorms (33%) show an above-average fraction of days with positive occurrence trends while 4 events (4.4%) are linked to negative trends (Fig. 3b and Extended Data Fig. S12). These statistics aggregate values on a continental level. A geographically-resolved picture highlights that the proportion of storms associated with patterns showing positive occurrence trends is larger in Continental/Northern Europe than in Southern Europe (Fig. 3b, e.g 40% in United Kingdom versus 0% in Italy). This is consistent with the pattern shown in Fig. 1a), which is reminiscent of the anomalies associated with destructive windstorms over Continental Europe found by[5].

In this paper, we identified the atmospheric circulation patterns over the North Atlantic and Europe that have become less or more frequent in the historical period. We focused on the changes in the occurrence of daily patterns, rather than on conventional weather regimes, climate indices or other aggregated patterns [6,17,25,30]. Our approach is fundamentally different from the latter in that we do not constraint our analysis to a fixed number of reference spatial patterns of some atmospheric field, but rather view each atmospheric pattern as unique and characterised by rare recurrences (a few % of all data in our analysis). We are thus able to isolate significant linear trends in the frequency of occurrence of specific, observed circulation patterns. The difference from previous studies is not only methodological, but also interpretative. For example, we find increasing occurrence of zonal flow patterns and decreasing occurrence of antizonal patterns over the North Atlantic during winter, which do not emerge from a conventional weather regime-based perspective[31,32].

Our method is flexible, and could for example be used as a complement to extreme event attribution studies conditioned on the circulation[33,34], otherwise known as the storyline approach[35]. The latter approach has been criticized for not taking into account the role of climate change-induced circulation changes[36], and we provide a readily applicable toolkit to address this problem. Our approach is not data or location-specific, and may be applied to different regions or datasets. This makes it well-suited as a tool to evaluate the consistency of dynamical trends in numerical simulations with those observed in reanalysis data. Our analysis does not enable to make a robust statement as to the potential role of natural variability in modulating the trends in atmospheric circulation pattern occurrence over the recent decades of anthropogenically-driven climate change. An analysis of climate modes of low-frequency variability highlights a statistical modulation of ENSO variability on trends in circulation pattern occurrence (see Extended Data and Extended Data Fig. S13), which should be taken into consideration when interpreting our results.

An important limitation of our study is that it assumes that the circulation patterns of interest have good analogues in the dataset being used (see Methods). This assumption is problematic in the presence of strong non-stationarities, which may lead to unprecedented atmospheric states. A theoretical advance would be to complement the analysis with a systematic investigation of analogue quality, based on the distance between a day and its analogues. Preliminary analyses to this effect show no long-term trends in analogue quality, yet some interannual variability which may relate to the above-discussed ENSO modulation. A second caveat is that the analysis of surface impacts through the EM-DAT and windstorms databases likely suffers from temporal and spatial inconsistencies in reporting — a common limitation of impacts data[37]. In our specific case, the partial reliance of the windstorms database on catalogues compiled for the scientific literature (see Methods), could alleviate the issue, but by no means completely resolves it.

We underscore that the temperature anomalies associated with increasingly frequent circulation patterns (Figs. 1e, 2e) are regionally comparable to or larger than the average global climate change (+1.2°C) with winter (summer) temperatures anomalies up to +5.7°C (+1.1°C). These results are obtained after detrending and deseasonalising the data, and are consistent with those obtained for the 500 hPa geopotential height in the Extended Data.

The circulation types we study, while rare (approximately 7% of all winter and summer days in our dataset), are associated with impactful extreme events, both deadly heatwaves and destructive windstorms. While these events are not exclusively caused by circulations changes, our results show that circulation changes cannot be neglected when evaluating the consequences of anthropogenic climate change or other sources of climatic variability on extreme weather events and their impacts.

Methods

Computing trends in the occurrence of atmospheric circulation patterns

For the computation of the trends in the occurrence of atmospheric circulation pattern analogues (which we hereafter refer to as "occurrence trends"), we use daily sea level pressure and 500hPa geopotential height data from the ERA5 reanalysis[26] over the period 01/01/1950 – 31/12/2021 (26,280 days). The data have a horizontal resolution of $0.25^\circ \times 0.25^\circ$, and we restrict our analysis to 80W – 50E and 22.5N – 70N. This corresponds to the North Atlantic and Europe, with a size of 200×530 grid cells. Part of the analysis was repeated on additional datasets (see Extended Data). For both the sea-level pressure and 500 hPa geopotential height data, we remove a grid point by grid point linear trend for the whole analysis period, and deseasonalise using a mean seasonal cycle computed by averaging over the same calendar days. The robust trends in the occurrence of atmospheric circulation patterns are computed as follows:

1. We select a daily sea-level pressure or 500 hPa geopotential height latitude–longitude maps, which we interpret as an atmospheric circulation pattern.

2. We compute the Euclidean distance between daily maps, taking each daily map in turn as reference state and computing its distance from all other maps in the dataset. We then define a high quantile q to select the analogues. We chose $q = 0.98$, meaning that we take as analogues the 2% closest fields to the target.

3. We divide the time interval of 73 years in 9 periods of roughly 8 years. We then count how many analogues N fall in each period t, obtaining $N(t)$ with $0 < t \leq 9$.

4. We perform a linear fit of $N(t)$ of the type $at + b$.

5. We estimate the upper and lower 95% confidence intervals (CI) of the a parameter of the fit using the Wald method[38]. If the lower and the upper bounds of the CI for a are positive (negative), we interpret this as a significant positive (negative) trend for the selected daily sea-level pressure or 500 hPa geopotential height map and quantile q. If the confidence interval contains zero, the trend is non-significant.

6. We test the sensitivity to the choice of quantile q by repeating the above steps for $q = 0.99, 0.995$ and retaining as daily maps with significant increasing (decreasing) occurrence trends only those having consistent (same sign AND significant) analogue occurrence trends for all three quantiles. These are the robust circulation patterns that are analysed in this paper. We additionally verify that the quality (i.e. distance) of analogues for these patterns is comparable to that for all other days in our dataset.

While analogues are a relatively common analysis approach in the atmospheric sciences, our methodology and its focus on trends is novel. It is further fundamentally different from conventional decompositions of the atmospheric variability, such as self-organsing maps[39], k-means clustering [40], Empirical Orthogonal Functions or others[41]. Indeed, we do not constraint our analysis to a fixed number of circulation patterns. The occurrence trends are thus identified for daily patterns rather than for a fixed pattern associated with a self-organising map or weather regime. Indeed, the computation of the analogues does not require introducing any specific decomposition bases, which in turn introduces arbitrary hyperparameters such as the number of components into which the atmospheric variability is partitioned. Moreover, we do not "create" reference fields that may have never been observed in the data by orthogonal decomposition, averaging or centroid computations. Our approach thus relies directly on the atmospheric variability present in the data, without adding an intermediate projection step.

Computation of Significant Circulation and Surface Anomalies

After identifying the circulation patterns with robust increasing or decreasing occurrence trends for the whole year, we produce composite anomalies for the patterns on days within the winter (DJF) and summer (JJA) months (without including their analogues) for several daily variables: sea-level pressure, 500 hPa geopotential height, horizontal 10m wind speed, horizontal 10m wind direction and precipitation rate. All these data are detrended and deseasonalised using the same procedure as for sea-level pressure and 500 hPa geopotential height. Significance for the geographical anomalies is estimated by using a bootstrap procedure (sample size $m = 500$) consisting in randomly drawing a number of days equal to the number of composites from the whole dataset regardless of the sign of the trend. The significance level is below the 5% and above the 95% percentiles of the bootstrap distribution at each grid point. Long term trends shown in the composites of Figs. 1–2 and Extended Data Figs. S2-S11 are computed by averaging, for each season, the spatial averages over all continental Europe (mask is given in Extended Data Fig. S1) for the patterns displaying occurrence trends. Years with missing observations are treated as NaNs. Significance for trends is estimated as previously described: by using the Wald method and looking at the sign of both the upper and lower bounds of the CI. CI trends are displayed in the legends of the relevant figure panels.

Computing impacts of atmospheric circulation patterns with positive occurrence trends

We take heat waves and cold spells from the EM-DAT disaster database[27]. We focus on events over Western-Central Europe (excluding e.g. Western Russia, outlying islands such as the Canary Islands etc.; Extended Data Fig. 1), excluding those heat waves and cold spells where no start and/or end day was provided, or which lasted only for one day. Dates included in several events were only counted once. Following these criteria, from a total of 34 heatwave and 66 cold spell episodes included in EM-DAT, we identified 228 days over 10 heatwaves and 480 days over 16 cold spells. Of the original 34 heatwave events, 3 were excluded because they were entirely outside Europe proper, 11 because they were missing start and/or end dates, 9 because a single day was assigned to the heatwave. Finally 2 heatwaves were merged into 1 because, even though they had different "disaster numbers" (i.e. unique identifiers of each disaster in EM-DAT), they had overlapping dates and occurred in geographically contiguous regions. Of the 66 cold spells, a relatively larger number is excluded due to being outside of Europe proper (13 events were only registered in Russia). An additional 35 are excluded due to missing or single-day dates. Finally, four events were merged into 2 because, even though they had different "disaster numbers", they had overlapping dates and occurred in geographically contiguous regions.

European Windstorms data is taken from an updated version of the storm database of[29] European Windstorms data is taken from an updated version of the storm database of[29], which originally covered the period 1948–2015. This database is largely based on the catalogues by[42] (arriving up to 1972) and[43] (arriving up to 2014). Additional storms have been integrated from the Wikipedia web-page https://en.wikipedia.org/wiki/List_of_European_windstorms because of their relevance in terms of human losses, damages or their profile in the media. We have only selected storms that have been analyzed by a meteorological office or research institute: a link to the documentation is provided together with each entry in the dataset. The dataset itself is available as Supplementary Data. Using publicly contributed databases as sources for scientific information is becoming a common practice in citizen science projects, which are gaining momentum in the geosciences[44,45]. Our database includes a total of 438 storm dates and 90 distinct storms or storm clusters. Extended Fig. S12 presents the database entries per country (a) and per time of occurrence (b).

The database is organized in four columns:

1. The day of occurrence in the format yyyymmdd;
2. The name(s) of the storm;
3. The countrie(s) or the region(s) affected;
4. A reference to a peer-reviewed article, a report or a press article describing the importance of the storm.

As a caveat to our methodology, we note that the increasing coverage of both meteorological instruments and technological means of information result in an increasing number of storms with time.

To determine whether a given extreme event is associated to circulation patterns with positive or negative occurrence trends, we first compute the fraction of days with positive occurrence trends within each heatwave or storm. We then compare these fractions to the average frequency of occurrence of circulation patterns with positive or negative occurrence trends within the 20 years centered on the heatwave or storm. This is because the frequency of occurrence of atmospheric circulation patterns with positive occurrence trends is by definition higher in the later part of the data than in the earlier years, such that each heatwave/storm should be compared to the period within which it occurs. Based on this comparison, we then separate events into groups which have an above or below-average fraction of daily analogues with either trend.

References

1. Forzieri, G. *et al.* Escalating impacts of climate extremes on critical infrastructures in europe. *Glob. environmental change* **48**, 97–107 (2018).
2. Sousa, P. M. *et al.* Distinct influences of large-scale circulation and regional feedbacks in two exceptional 2019 european heatwaves. *Commun. Earth & Environ.* **1**, 1–13 (2020).
3. Lehmann, J. & Coumou, D. The influence of mid-latitude storm tracks on hot, cold, dry and wet extremes. *Sci. reports* **5**, 1–9 (2015).
4. Zanardo, S., Nicotina, L., Hilberts, A. G. & Jewson, S. P. Modulation of economic losses from european floods by the north atlantic oscillation. *Geophys. Res. Lett.* **46**, 2563–2572 (2019).
5. Hanley, J. & Caballero, R. The role of large-scale atmospheric flow and rossby wave breaking in the evolution of extreme windstorms over europe. *Geophys. Res. Lett.* **39** (2012).

6. Cattiaux, J., Peings, Y., Saint-Martin, D., Trou-Kechout, N. & Vavrus, S. J. Sinuosity of midlatitude atmospheric flow in a warming world. *Geophys. Res. Lett.* **43**, 8259–8268 (2016).

7. Horton, R. M., Mankin, J. S., Lesk, C., Coffel, E. & Raymond, C. A review of recent advances in research on extreme heat events. *Curr. Clim. Chang. Reports* **2**, 242–259 (2016).

8. Mann, M. E. *et al.* Projected changes in persistent extreme summer weather events: The role of quasi-resonant amplification. *Sci. advances* **4**, eaat3272 (2018).

9. Cohen, J. *et al.* Divergent consensuses on arctic amplification influence on midlatitude severe winter weather. *Nat. Clim. Chang.* **10**, 20–29 (2020).

10. Riboldi, J., Lott, F., d'Andrea, F. & Rivière, G. On the linkage between rossby wave phase speed, atmospheric blocking, and arctic amplification. *Geophys. Res. Lett.* **47**, e2020GL087796 (2020).

11. Coumou, D., Lehmann, J. & Beckmann, J. The weakening summer circulation in the northern hemisphere mid-latitudes. *Science* **348**, 324–327 (2015).

12. Coumou, D., Di Capua, G., Vavrus, S., Wang, L. & Wang, S. The influence of arctic amplification on mid-latitude summer circulation. *Nat. Commun.* **9**, 1–12 (2018).

13. Routson, C. C. *et al.* Mid-latitude net precipitation decreased with arctic warming during the holocene. *Nature* **568**, 83–87 (2019).

14. Kornhuber, K. *et al.* Extreme weather events in early summer 2018 connected by a recurrent hemispheric wave-7 pattern. *Environ. Res. Lett.* **14**, 054002 (2019).

15. Röthlisberger, M., Frossard, L., Bosart, L. F., Keyser, D. & Martius, O. Recurrent synoptic-scale rossby wave patterns and their effect on the persistence of cold and hot spells. *J. Clim.* **32**, 3207–3226 (2019).

16. Hassanzadeh, P., Kuang, Z. & Farrell, B. F. Responses of midlatitude blocks and wave amplitude to changes in the meridional temperature gradient in an idealized dry gcm. *Geophys. Res. Lett.* **41**, 5223–5232 (2014).

17. Horton, D. E. *et al.* Contribution of changes in atmospheric circulation patterns to extreme temperature trends. *Nature* **522**, 465–469 (2015).

18. Mann, M. E. *et al.* Influence of anthropogenic climate change on planetary wave resonance and extreme weather events. *Sci. reports* **7**, 1–12 (2017).

19. Jézéquel, A., Yiou, P., Radanovics, S. & Vautard, R. Analysis of the exceptionally warm december 2015 in france using flow analogues. *Bull. Am. Meteorol. Soc.* (2017).

20. Jézéquel, A. *et al.* Trends of atmospheric circulation during singular hot days in europe. *Environ. Res. Lett.* **13**, 054007 (2018).

21. Rogers, C. D., Kornhuber, K., Perkins-Kirkpatrick, S. E., Loikith, P. C. & Singh, D. Sixfold increase in historical northern hemisphere concurrent large heatwaves driven by warming and changing atmospheric circulations. *J. Clim.* **35**, 1063–1078 (2022).

22. Perkins-Kirkpatrick, S. & Lewis, S. Increasing trends in regional heatwaves. *Nat. communications* **11**, 1–8 (2020).

23. Vicente-Serrano, S. M. & López-Moreno, J. I. The influence of atmospheric circulation at different spatial scales on winter drought variability through a semi-arid climatic gradient in northeast spain. *Int. J. Climatol. A J. Royal Meteorol. Soc.* **26**, 1427–1453 (2006).

24. Barlow, M. *et al.* North american extreme precipitation events and related large-scale meteorological patterns: a review of statistical methods, dynamics, modeling, and trends. *Clim. Dyn.* **53**, 6835–6875 (2019).

25. Corti, S., Molteni, F. & Palmer, T. Signature of recent climate change in frequencies of natural atmospheric circulation regimes. *Nature* **398**, 799–802 (1999).

26. Hersbach, H. *et al.* Era-20cm: A twentieth-century atmospheric model ensemble. *Q. J. Royal Meteorol. Soc.* **141**, 2350–2375 (2015).

27. Guha-Sapir, D. Em-dat: The emergency events database–université catholique de louvain (ucl)–cred, brussels, belgium (2017).

28. Fouillet, A. *et al.* Excess mortality related to the august 2003 heat wave in france. *Int. archives occupational environmental health* **80**, 16–24 (2006).

29. Faranda, D., Messori, G. & Yiou, P. Dynamical proxies of north atlantic predictability and extremes. *Sci. reports* **7**, 1–10 (2017).

30. Cassou, C. & Cattiaux, J. Disruption of the european climate seasonal clock in a warming world. *Nat. Clim. Chang.* **6**, 589–594 (2016).

31. Iles, C. & Hegerl, G. Role of the north atlantic oscillation in decadal temperature trends. *Environ. Res. Lett.* **12**, 114010 (2017).

32. Matsueda, M. & Palmer, T. Estimates of flow-dependent predictability of wintertime euro-atlantic weather regimes in medium-range forecasts. *Q. J. Royal Meteorol. Soc.* **144**, 1012–1027 (2018).

33. Meredith, E. P., Semenov, V. A., Maraun, D., Park, W. & Chernokulsky, A. V. Crucial role of black sea warming in amplifying the 2012 krymsk precipitation extreme. *Nat. Geosci.* **8**, 615–619 (2015).

34. Trenberth, K. E., Fasullo, J. T. & Shepherd, T. G. Attribution of climate extreme events. *Nat. Clim. Chang.* **5**, 725–730 (2015).

35. Shepherd, T. G. A common framework for approaches to extreme event attribution. *Curr. Clim. Chang. Reports* **2**, 28–38 (2016).

36. Otto, F. E. *et al.* The attribution question. *Nat. Clim. Chang.* **6**, 813–816 (2016).

37. Gall, M., Borden, K. A. & Cutter, S. L. When do losses count? six fallacies of natural hazards loss data. *Bull. Am. Meteorol. Soc.* **90**, 799–810 (2009).

38. Stein, C. & Wald, A. Sequential confidence intervals for the mean of a normal distribution with known variance. *The Annals Math. Stat.* 427–433 (1947).

39. Kohonen, T. The self-organizing map. *Proc. IEEE* **78**, 1464–1480 (1990).

40. Dunn, O. J. Multiple comparisons among means. *J. Am. statistical association* **56**, 52–64 (1961).

41. Hannachi, A., Straus, D. M., Franzke, C. L., Corti, S. & Woollings, T. Low-frequency nonlinearity and regime behavior in the northern hemisphere extratropical atmosphere. *Rev. Geophys.* **55**, 199–234 (2017).

42. Lamb, H. H. British isles weather types and a register of the daily sequence of circulation patterns 1861-1971. (1972).

43. Roberts, J. *et al.* The xws open access catalogue of extreme european windstorms from 1979 to 2012. *Nat. Hazards Earth Syst. Sci.* **14**, 2487–2501 (2014).

44. Fritz, S. *et al.* Geo-wiki: An online platform for improving global land cover. *Environ. Model. & Softw.* **31**, 110–123 (2012).

45. Sparrow, S. *et al.* Openifs@ home version 1: a citizen science project for ensemble weather and climate forecasting. *Geosci. Model. Dev.* **14**, 3473–3486 (2021).

Acknowledgement

D.Faranda, M. Vrac, P. Yiou received funding under the European Union's Horizon 2020 research and innovation programme (Grant agreement No. 101003469, XAIDA). D. Faranda, G. Messori and P. Yiou received funding under the European Union's Horizon 2020 research and innovation programme, Marie Skłodowska-Curie (Grant agreement No. 956396, EDIPI). G. Messori received funding from the European Research Council (ERC) under the European Union's Horizon 2020 research and innovation programme (Grant agreement No. 948309, CENAE). D. Faranda acknowledges the support of the ANR-TERC grant BOREAS and the LEFE-MANU-INSU-CNRS grant DINCLIC. P. Yiou was supported by the French ANR grant No. ANR-20-CE01-0008-01 (SAMPRACE). All authors thank three anonymous reviewers and the editor for their support in improving the study.

Author contributions

D.F. conceived the study, performed the bulk of the analysis and compiled the European windstorm database. G.M performed the analysis on the EM-DAT database and contributed to compiling the European windstorm database. D.F and G.M, wrote and revised the manuscript. D.F., G.M., A.J., M.V. and P.Y. read and integrated the manuscript.

Competing Interests

The authors report no conflict of interest.

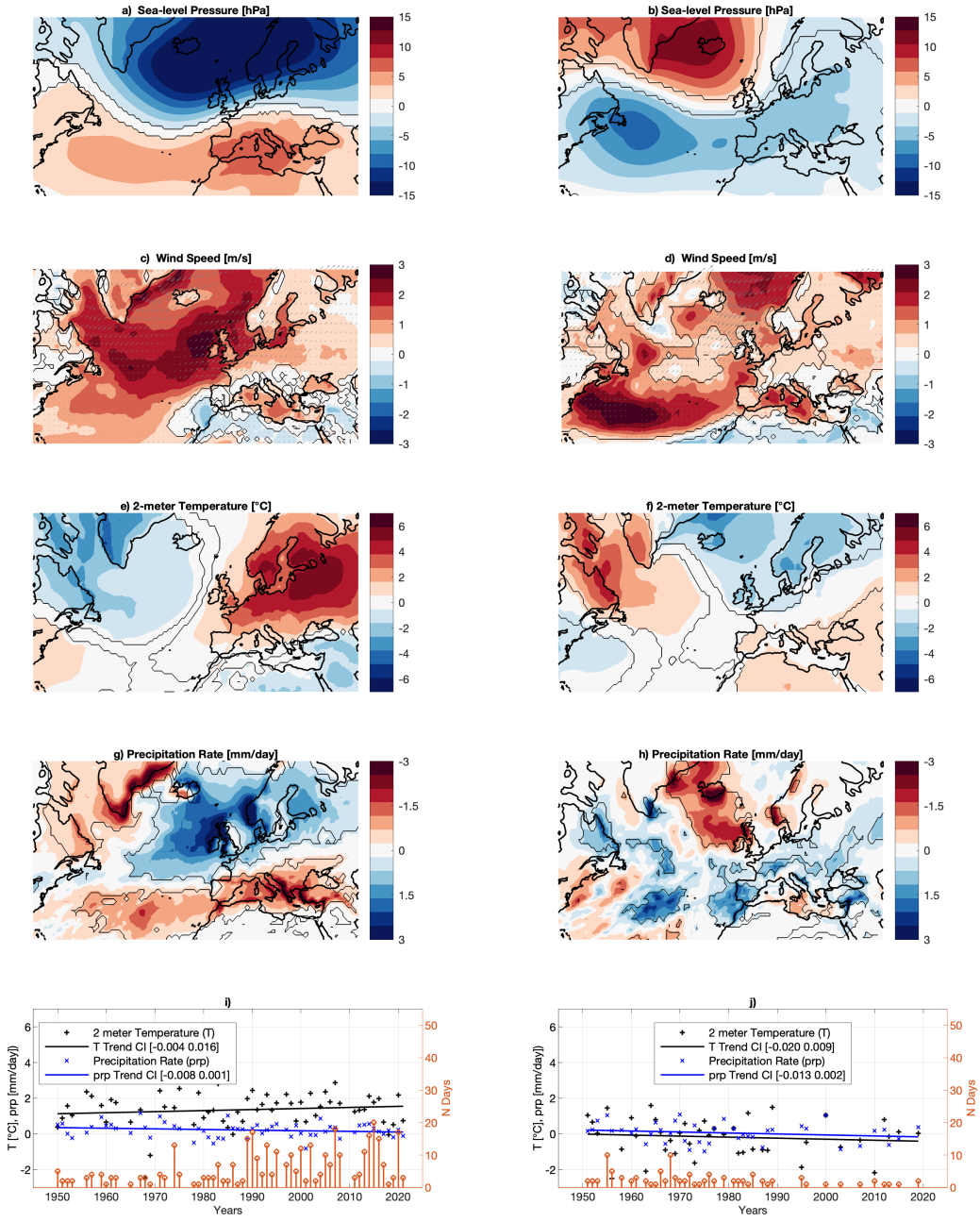

Figure 1. Sea-level pressure wintertime atmospheric circulation patterns with significant occurrence trends and associated surface anomalies: Composite anomalies of DJF sea-level pressure (a,b), 10m horizontal wind direction and intensity (c,d), 2-meter temperatures (e,f) and precipitation rates (g,h) for days with increasing (a,c,e,g) or decreasing (b,d,f,h) occurrence trends. In the composites (a–h), contours indicate regions with changes significant at the 5% level, computed with a bootstrap sample size of 500. Spatial averages of seasonal temperature anomalies (black) and precipitation rates (blue) during the days with increasing (i) or decreasing (j) occurrence trends and count of days displaying the corresponding occurrence trend (orange stems) during DJF. Solid lines represent linear trends of the spatial averages with the 95% confidence intervals of the two linear fits in each panel shown in the legends. The averages in (i), (j) are computed on all European land points (domain shown in Extended Data Fig. S1).

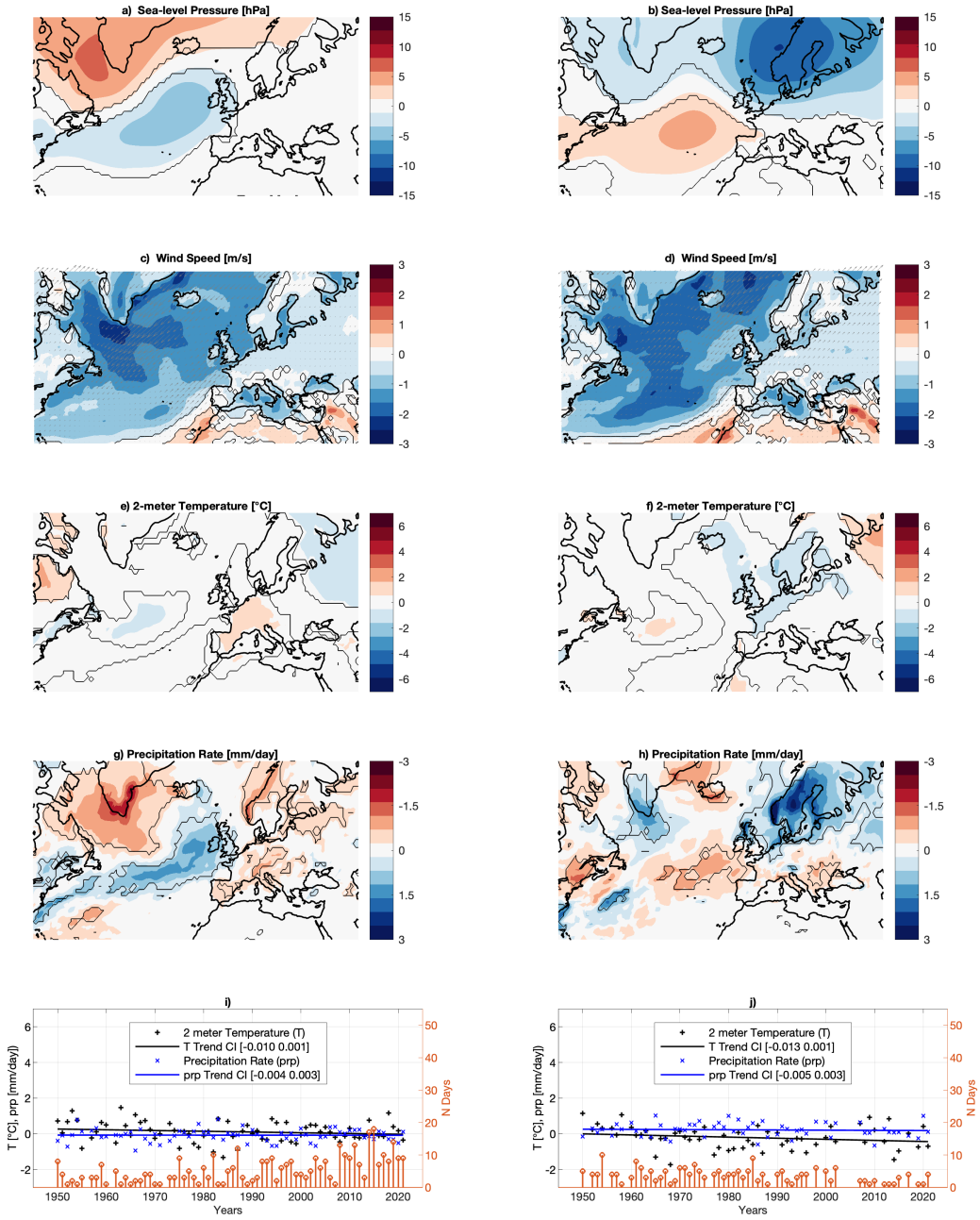

Figure 2. Sea-level pressure summertime atmospheric circulation patterns with significant occurrence trends and associated surface anomalies: As in Fig. 1, but for JJA.

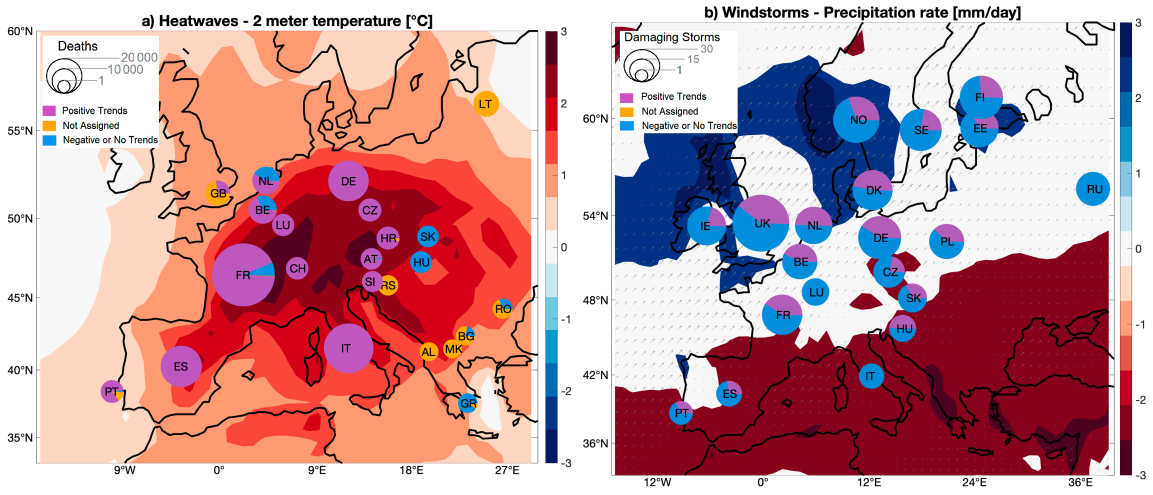

Figure 3. Impacts of changing atmospheric circulation patterns in terms of heatwave casualties and European Windstorms. (a) The size of the pie chart for each country shows the total number of heatwave excess deaths as recorded in the EM-DAT database for the whole year. The purple slices show the fraction of excess deaths associated with heatwaves showing an above-average frequency of circulation patterns with a positive occurrence trend. The yellow slices show the excess deaths associated with heatwaves that we excluded from our analysis (see Methods). Finally, the blue slices show the corresponding fractions for heatwaves showing circulation patterns with no or negative occurrence trends. The shading on the geographical map shows the temperature anomalies (°C) during the 228 heatwave days retained for analysis. (b) The size of the pie chart for each country shows the total number of destructive windstorms in the storm database for the whole year (see Methods). The purple slices show the fraction of storms showing an above-average frequency of circulation patterns with a positive occurrence trend. The blue slices show the corresponding fraction for storms showing analogues with no or negative occurrence trends. The shading on the geographical map shows the precipitation anomalies (mm day^{-1}) during the 438 windstorm days retained for analysis; vectors show 10m wind anomalies (m s^{-1}).

Extended Data for: Atmospheric circulation compounds anthropogenic warming and its impacts in Europe

Davide Faranda[1,2,3,*], Gabriele Messori[4,5], Aglae Jezequel[3,6], Mathieu Vrac[1], and Pascal Yiou[1]

[1]Laboratoire des Sciences du Climat et de l'Environnement, CEA Saclay l'Orme des Merisiers, UMR 8212 CEA-CNRS-UVSQ, Université Paris-Saclay & IPSL, 91191, Gif-sur-Yvette, France
[2]London Mathematical Laboratory, 8 Margravine Gardens, London, W6 8RH, UK
[3]LMD/IPSL, Ecole Normale Superieure, PSL research University, 75005, Paris, France
[4]Department of Earth Sciences, Uppsala University, and Centre of Natural Hazards and Disaster Science (CNDS), Uppsala, 752 36, Sweden
[5]Department of Meteorology and Bolin Centre for Climate Research, Stockholm University, 106 91, Stockholm, Sweden
[6]Ecole des Ponts, Marne-la-Vallée, France
[*]davide.faranda@lsce.ipsl.fr

ABSTRACT

The extended data contain: i) additional text and references, ii) 2 additional figures

Use of additional datasets

In addition to the ERA5 data used in the main text, we have repeated the computation of occurrence trends of atmospheric circulation patterns using sea-level pressure from the NCEP/NCAR reanalysis[1] (Figs. S2, S3 and 2m-temperature and precipitation from E-OBS v25.0e over land (Figs. S4, S5). Both datasets cover the same period as the main analysis, namely 01/01/1950 – 31/12/2021. The NCEP/NCAR data has a horizontal resolution of $2.5^\circ \times 2.5^\circ$, while the E-OBS v25.0e data has a horizontal resolution of $0.25^\circ \times 0.25^\circ$. We restrict our analysis to the same 80W – 50E and 22.5N – 70N domain used in the main text. Figures S2, S4 and S3, S5 correspond respectively to Figs. 1 and 2 computed for ERA5. Allowing for the different spatial resolutions of the datasets, which result in some modulation of the intensity of the anomalies, the corresponding patterns in all variables and seasons closely resemble each other. The fact that very different datasets provide the same conclusions supports the robustness of our analysis.

Analysis on sea-level pressure and 500 hPa geopotential height

In winter we note a very close resemblance of the 500 hPa geopotential height and sea-level pressure large-scale patterns for days with increasing occurrence trends. In both cases, the anomaly structure is an NAO-like meridional dipole favouring an intensified zonal flow. This leads to very similar surface anomalies (cf. Figs. 1a, c, e, g and S10a, c, e, g). For the wintertime decreasing occurrence trends, the 500 hPa geopotential height pattern has a marked meridional and quadripolar structure, while the sea-level pressure pattern is chiefly dipolar and anti-zonal. The surface anomalies over Europe are regionally different, although especially for precipitation some of the large-scale features are comparable (cf. Figs. 1b, d, f, h and S10b, d, f, h). A similar picture emerges for summer (Figs. 2 and S11). The large-scale patterns for days with increasing occurrence trends are broadly similar: both variables display a mid-Atlantic trough and a zonally extended band of positive anomalies in the northernmost part of the domain. We nonetheless note some meridional shift in the anomaly poles and the fact that 500 hPa geopotential height shows larger positive anomalies over Scandinavia. The patterns for decreasing occurrence trends again show larger differences. In the case of sea-level pressure, there is a dipolar pattern with the positive pole to the North of the Azores and the negative pole over Scandinavia. The 500 hPa geopotential height anomaly pattern is wave-like. This is to some extent also mirrored in the surface anomalies (cf. Figs. 2b, d, f, h and S11b, d, f, h). The scale would appear comparable to the wave-5 pattern of[2], although the surface temperature anomalies do not match those of the latter study. The pattern also

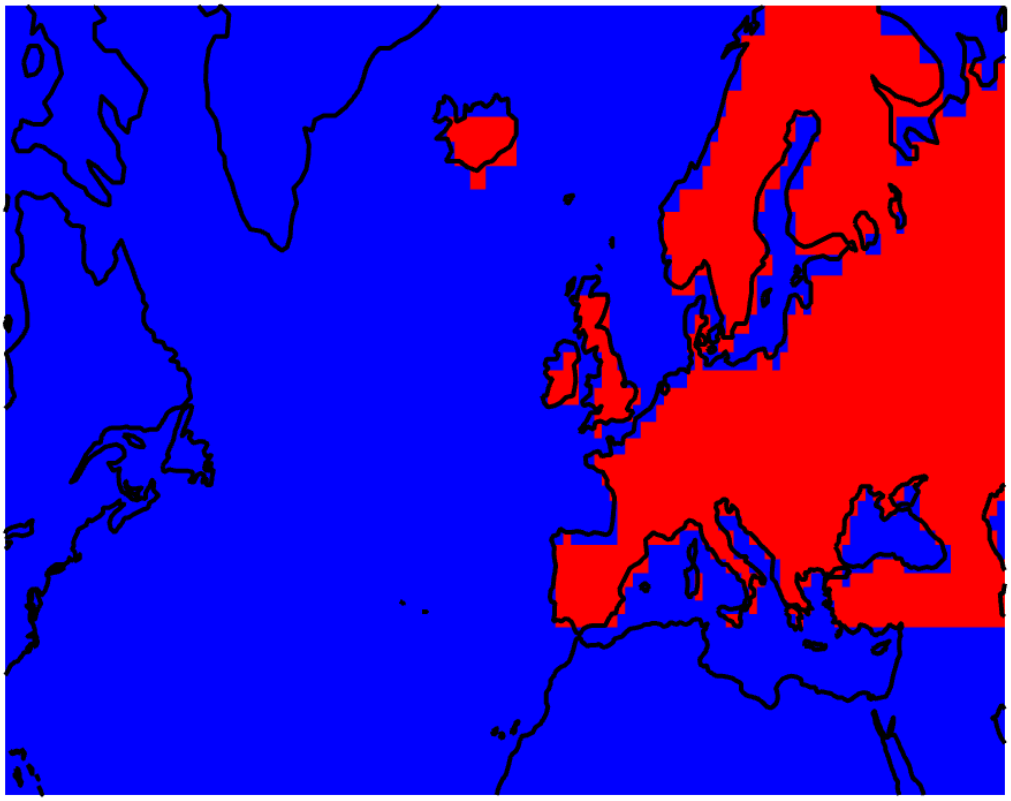

Figure S1. European mask used to compute timeseries of continental European data: Red shading shows the gridboxes used to compute timeseries of continental European data shown in Figs. 1i, j and 2i, j.

resembles the Node 7 500 hPa geopotential height pattern shown in[3], although the latter study finds that this pattern has a significantly increasing occurrence trend over the historical period, contrary to what we find in our analysis. The regional North Atlantic view we take may explain part of the discrepancy with the circumhemispheric wave view of[2,3].

Modulation of circulation pattern occurrences by natural variability

The atmospheric circulation pattern occurrence trends we identified in our analysis may be modulated by natural variability. To investigate this, we have analysed the correspondence between atmospheric circulation pattern occurrence trends and the Atlantic Multidecadal Oscillation (AMO) and El Nino–Southern Oscillation (ENSO) as diagnosed through the Nino 3.4 index. Specifically, we have tested whether days with positive occurrence trends correspond to anomalous ENSO or AMO values and whether high or low ENSO or AMO values favour positive, negative or neutral occurrence trends. In all cases, we have conducted the analysis using monthly indices computed from the NOAA/ERSSTv5 dataset[4] and retrieved from KNMI's climate explorer. The Nino 3.4 timeseries is normalised over the 1981–2010 period, while the AMO timeseries is normalised over the 1971–2010 period, meaning that they have a non-zero average over the analysis period we consider. The Nino 3.4 index has shown an upward trend in recent decades [5,6], something which we also see in our data. The AMO index also shows a weak trend. We have therefore conducted our analysis on both the raw and linearly detrended timeseries (the latter being centred on zero due to the detrending process). We see no significant association between atmospheric circulation pattern occurrence trends and the AMO (not shown). On the contrary, there is a clear association between ENSO variability and atmospheric circulation pattern occurrence trends. Nino 3.4 values are significantly positive (negative) for days with positive (negative) occurrence trends (Fig. S13a,b). Similarly, days with positive (negative) occurrence trends show a clear preference for months in the upper (lower) tertiles of the Nino 3.4 distribution (Fig. S13c,d). The above holds for both the raw and detrended Nino 3.4

timeseries, although the result in Fig. S13c,d are stronger for the undetrended ENSO timeseries.

We thus conclude that there appears to be a statistical modulation of ENSO variability on trends in the occurrence of atmospheric circulation patterns in the North Atlantic sector, and that the association between positive (negative) ENSO phases and days with positive (negative) occurrence trends is stronger if the long-term ENSO trend is taken into account. Focussing on days with positive occurrence trends, during winter we hypothesise that this may be linked to the NAO-like footprint of ENSO on North Atlantic sea-level pressure[7]. During summer the picture is not as clear, and recent work has found only weak relations between ENSO and the summer NAO[8].

Notwithstanding the possible low-frequency modulation of the atmospheric circulation pattern occurrence trends by internal climate variability, the patterns with increasing or decreasing occurrence trends that we identify appear stable throughout the analysis period. Figs. S6–S9 show the occurrence trend analysis for the first or last 20% of circulation pattern occurrences. With the exception of circulation patterns with decreasing occurrence trends in winter, which have a very small sample size, there is very little difference between the two timeperiods considered.

References

1. Kalnay, E. *et al.* The ncep/ncar 40-year reanalysis project. *Bull. Am. meteorological Soc.* **77**, 437–472 (1996).
2. Kornhuber, K. *et al.* Amplified rossby waves enhance risk of concurrent heatwaves in major breadbasket regions. *Nat. Clim. Chang.* **10**, 48–53 (2020).
3. Rogers, C. D., Kornhuber, K., Perkins-Kirkpatrick, S. E., Loikith, P. C. & Singh, D. Sixfold increase in historical northern hemisphere concurrent large heatwaves driven by warming and changing atmospheric circulations. *J. Clim.* **35**, 1063–1078 (2022).
4. Huang, B. *et al.* Extended reconstructed sea surface temperature, version 5 (ersstv5): upgrades, validations, and intercomparisons. *J. Clim.* **30**, 8179–8205 (2017).
5. L'Heureux, M. L., Collins, D. C. & Hu, Z.-Z. Linear trends in sea surface temperature of the tropical pacific ocean and implications for the el niño-southern oscillation. *Clim. Dyn.* **40**, 1223–1236 (2013).
6. L'Heureux, M. L., Lee, S. & Lyon, B. Recent multidecadal strengthening of the walker circulation across the tropical pacific. *Nat. Clim. Chang.* **3**, 571–576 (2013).
7. Mezzina, B., García-Serrano, J., Bladé, I. & Kucharski, F. Dynamics of the enso teleconnection and nao variability in the north atlantic–european late winter. *J. Clim.* **33**, 907–923 (2020).
8. Paciorek, C. J., Stone, D. A. & Wehner, M. F. Quantifying statistical uncertainty in the attribution of human influence on severe weather. *Weather. climate extremes* **20**, 69–80 (2018).

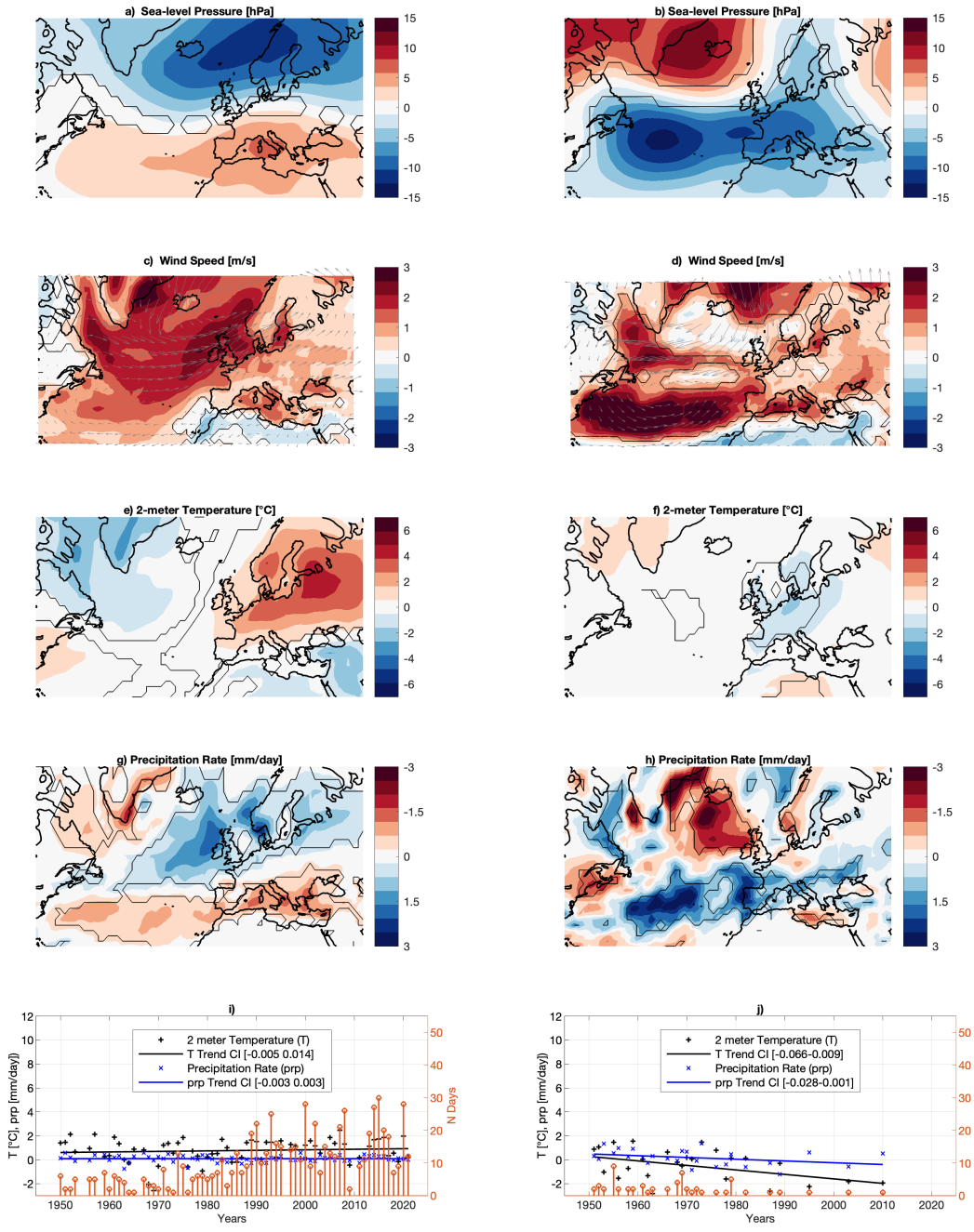

Figure S2. Sea-level pressure wintertime atmospheric circulation patterns with significant occurrence trends and associated surface anomalies: As in Fig. 1, but for NCEP-NCAR reanalysis data.

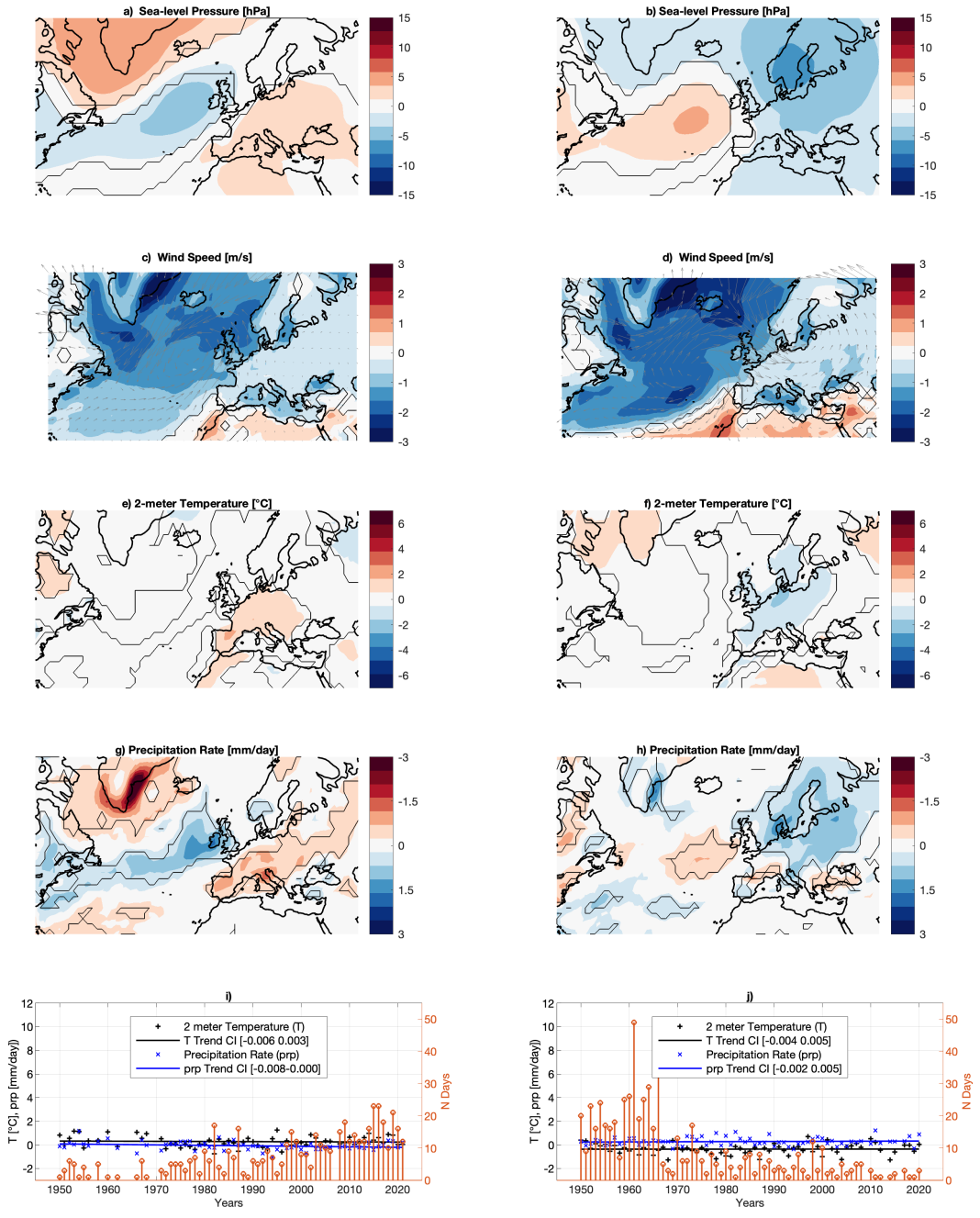

Figure S3. Sea-level pressure summertime atmospheric circulation patterns with significant occurrence trends and associated surface anomalies: As in Fig. 2, but for NCEP-NCAR reanalysis data.

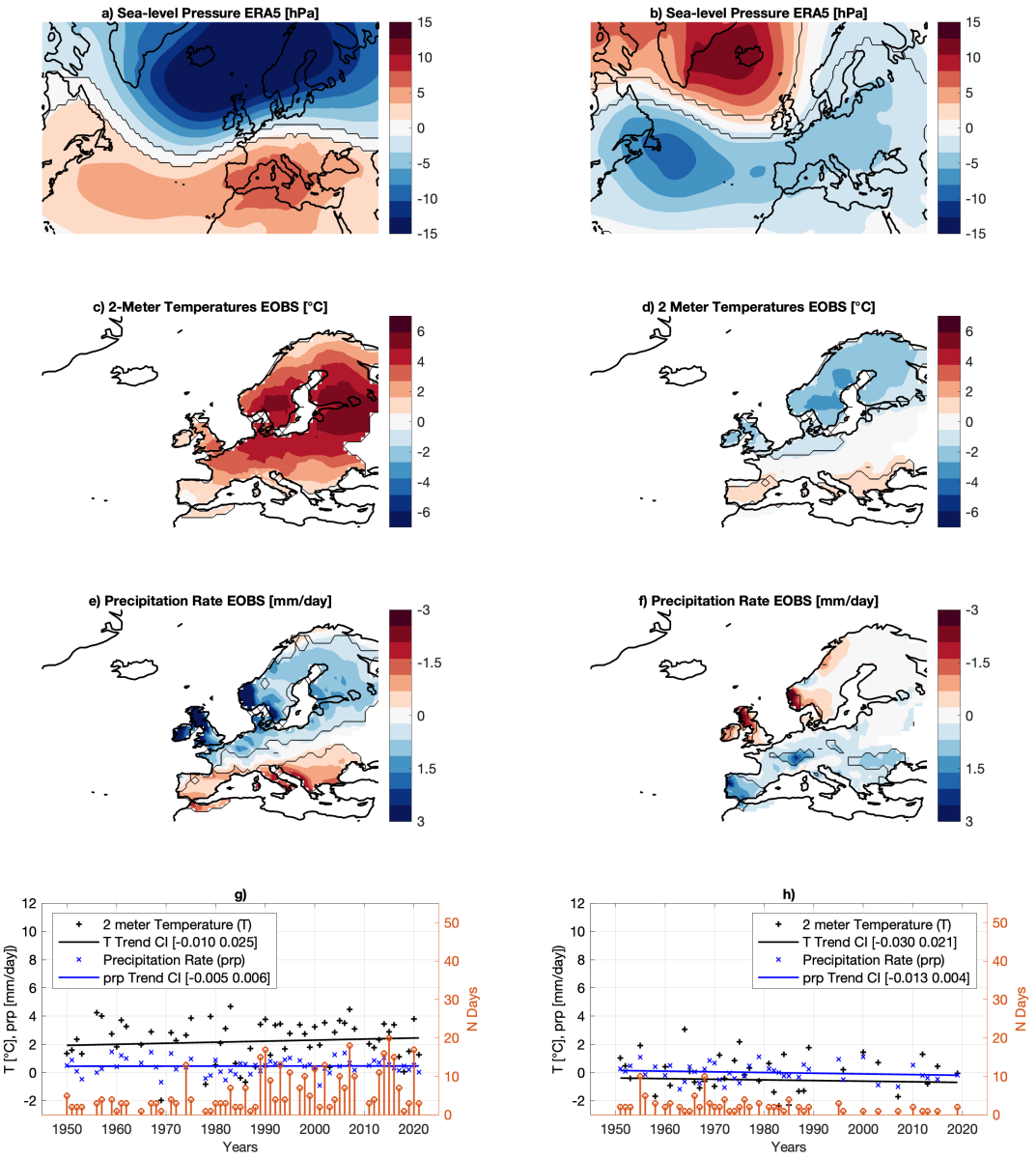

Figure S4. Sea-level pressure wintertime atmospheric circulation patterns with significant occurrence trends and associated surface anomalies: As in Fig. 1, but for ERA5 sea-level pressure data (a, b) and E-OBS temperature and precipitation (c–f). The figure does not include wind data.

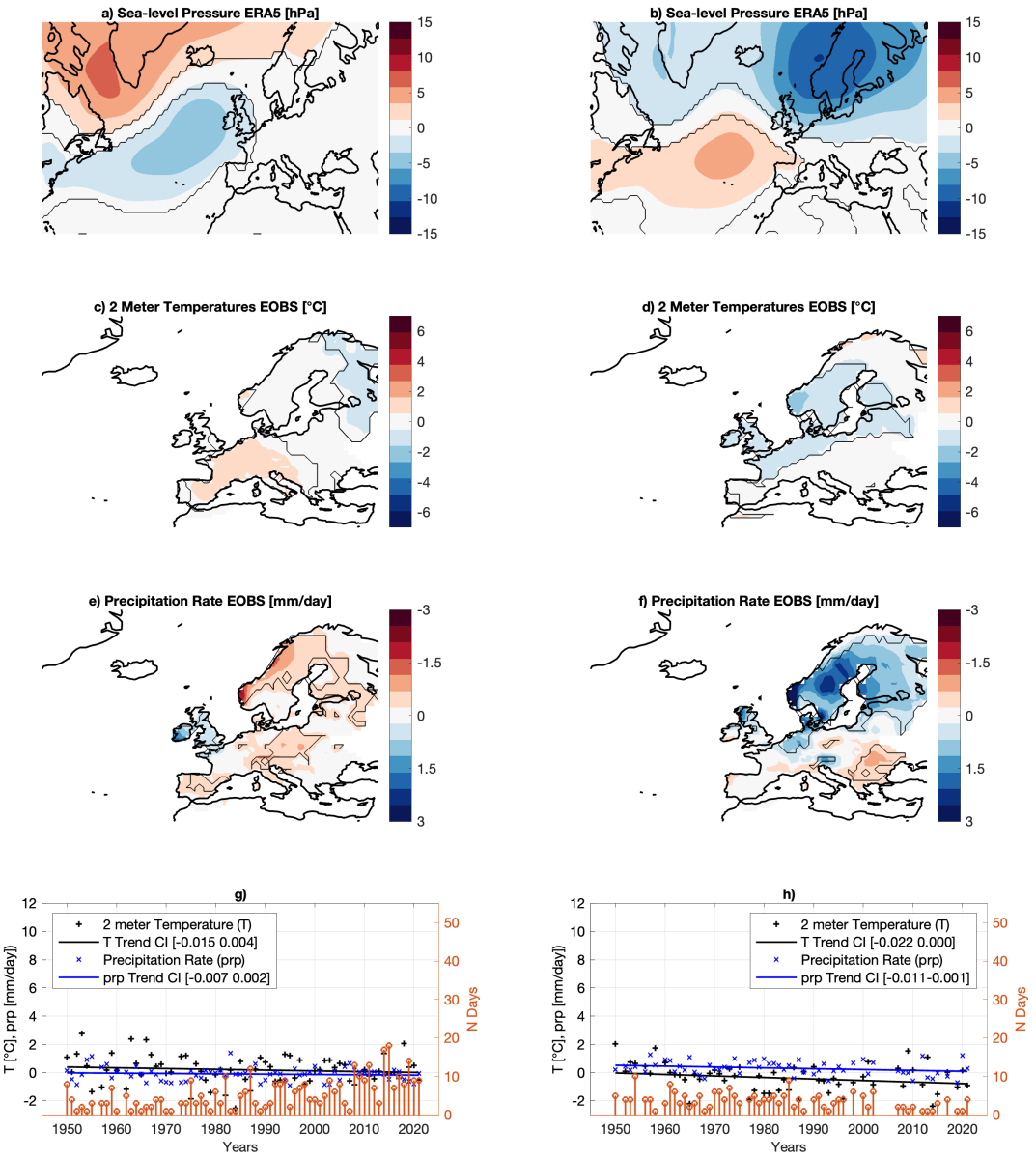

Figure S5. Sea-level pressure summertime atmospheric circulation patterns with significant occurrence trends and associated surface anomalies: As in Fig. 2, but for ERA5 sea-level pressure data data (a, b) and E-OBS 2-metre temperature and precipitation (c–f). The figure does not include wind data.

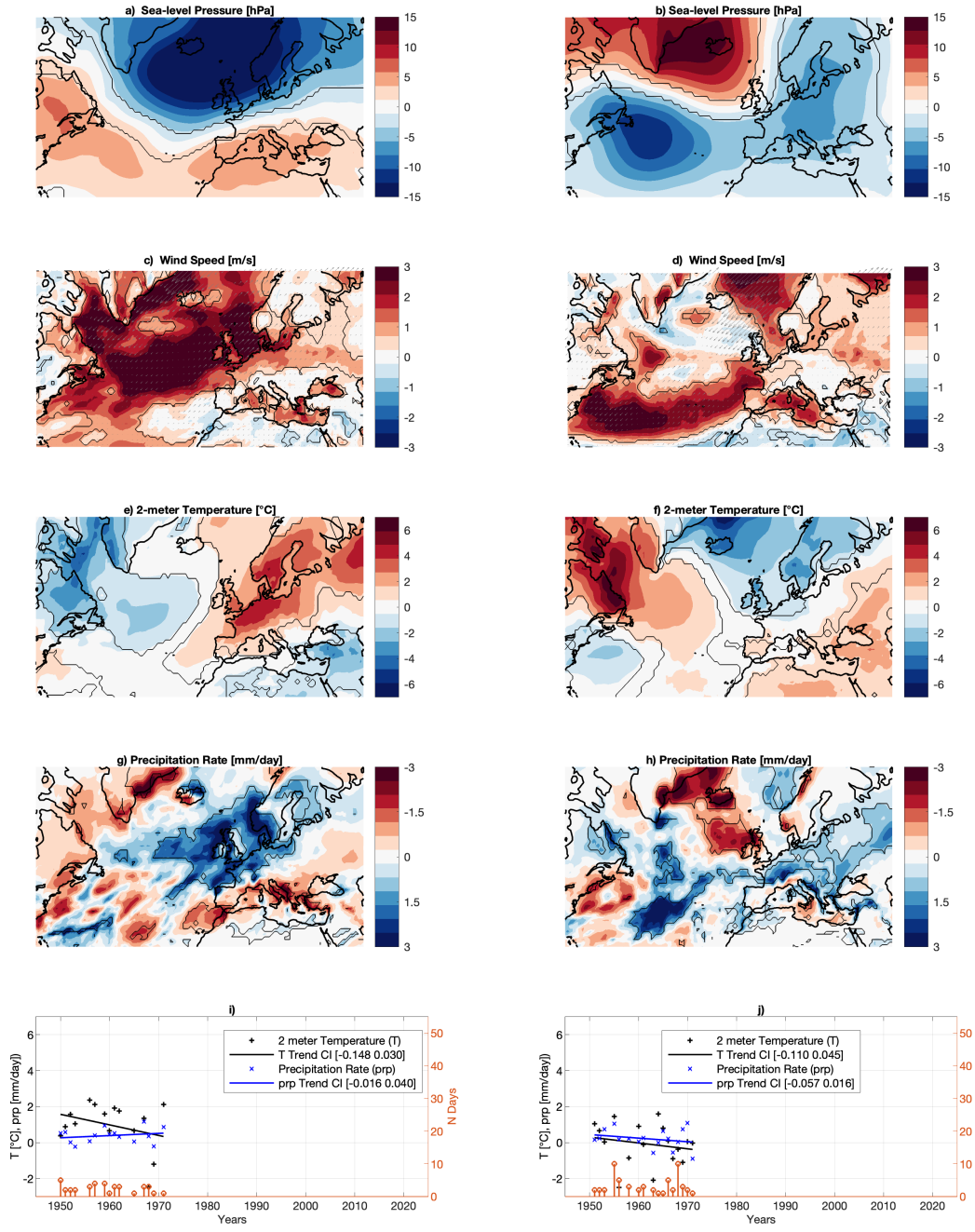

Figure S6. First 20% of the sea-level pressure wintertime atmospheric circulation patterns with significant occurrence trends and associated surface anomalies: As in Fig. 1, but for the (chronologically) earliest 20% of sea-level pressure wintertime atmospheric circulation patterns displaying significant occurrence trends.

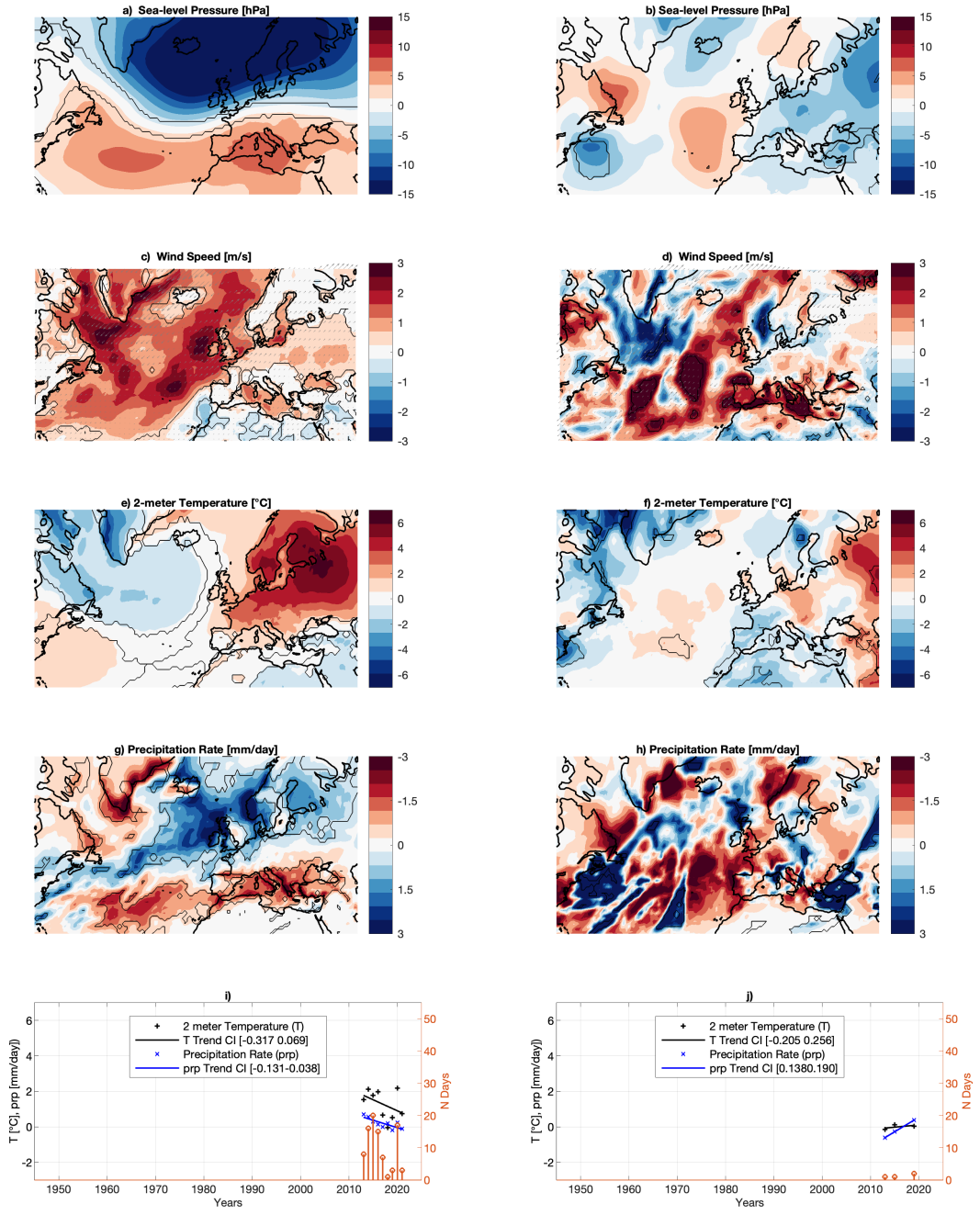

Figure S7. Last 20% of the sea-level pressure wintertime atmospheric circulation patterns with significant occurrence trends and associated surface anomalies: As in Fig. 1, but for the (chronologically) latest 20% of sea-level pressure wintertime atmospheric circulation patterns displaying significant occurrence trends.

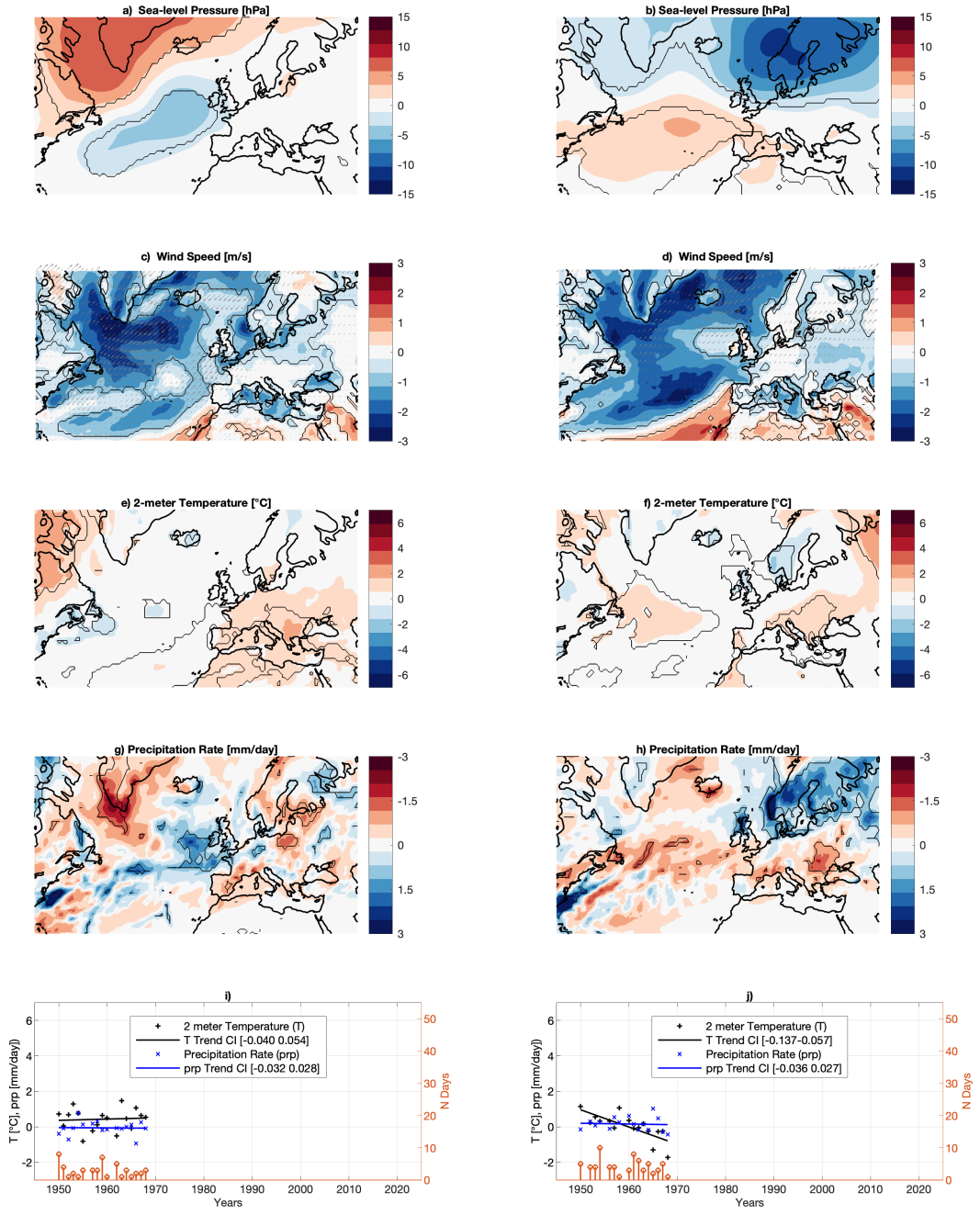

Figure S8. First 20% of the sea-level pressure summertime atmospheric circulation patterns with significant occurrence trends and associated surface anomalies: As in Fig. 2, but for the (chronologically) earliest 20% of sea-level pressure summertime atmospheric circulation patterns displaying significant occurrence trends.

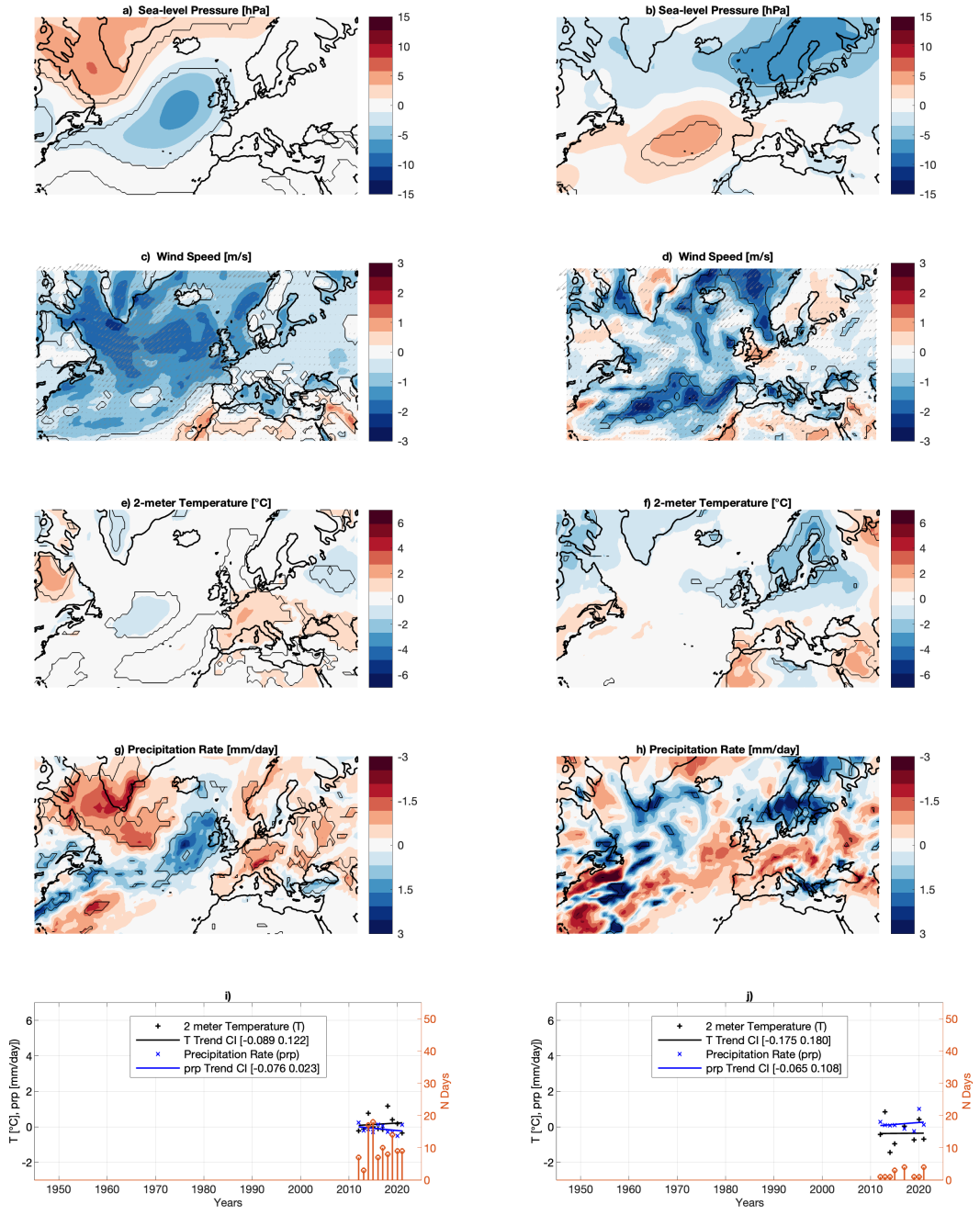

Figure S9. Last 20% of the sea-level pressure summertime atmospheric circulation patterns with significant occurrence trends and associated surface anomalies: As in Fig. 2, but for the (chronologically) latest 20% of sea-level pressure summertime atmospheric circulation patterns displaying significant occurrence trends.

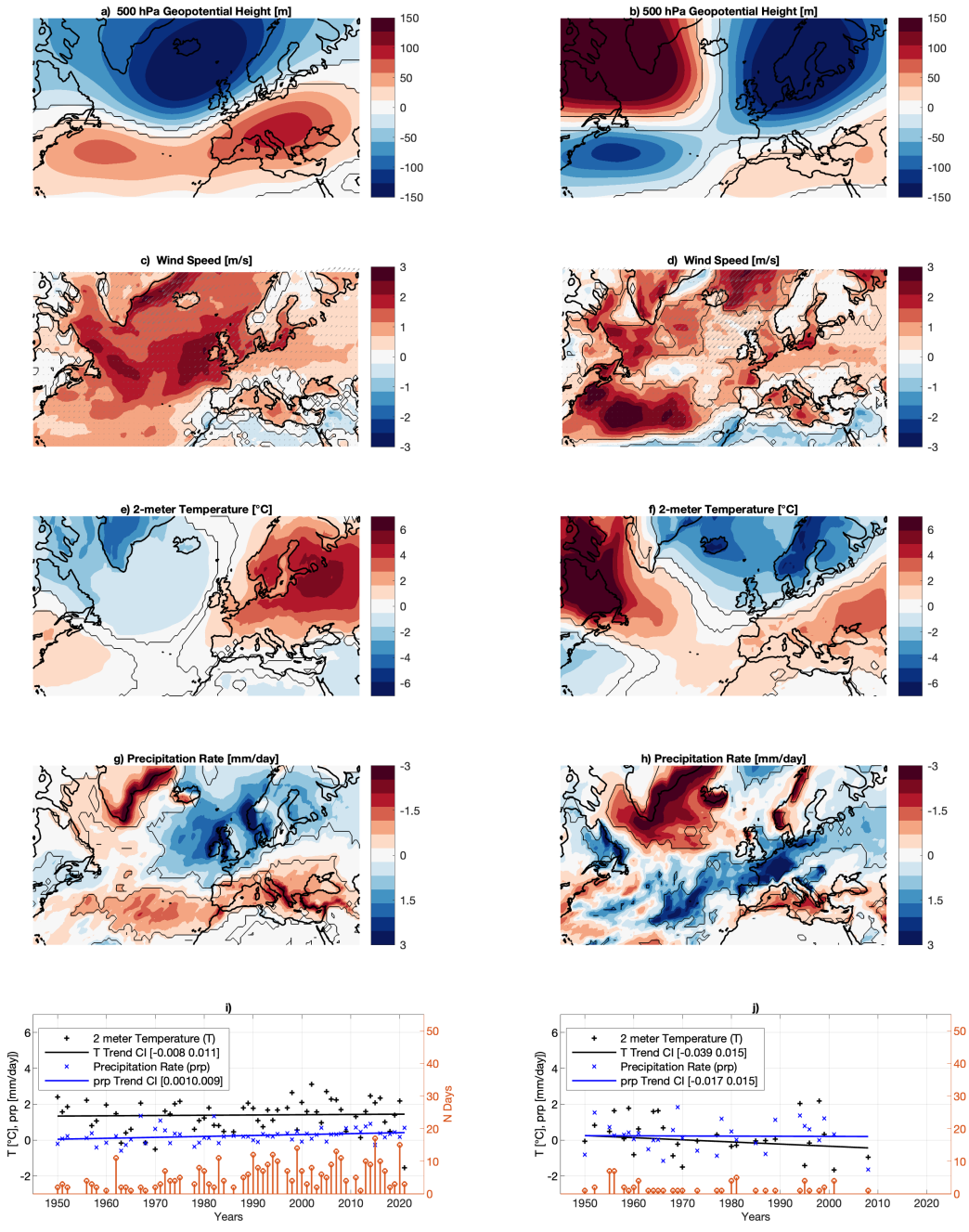

Figure S10. 500 hPa geopotential height wintertime atmospheric circulation patterns with significant occurrence trends and associated surface anomalies: As in Fig. 1, but for 500 hPa geopotential height for ERA5 data (a,b).

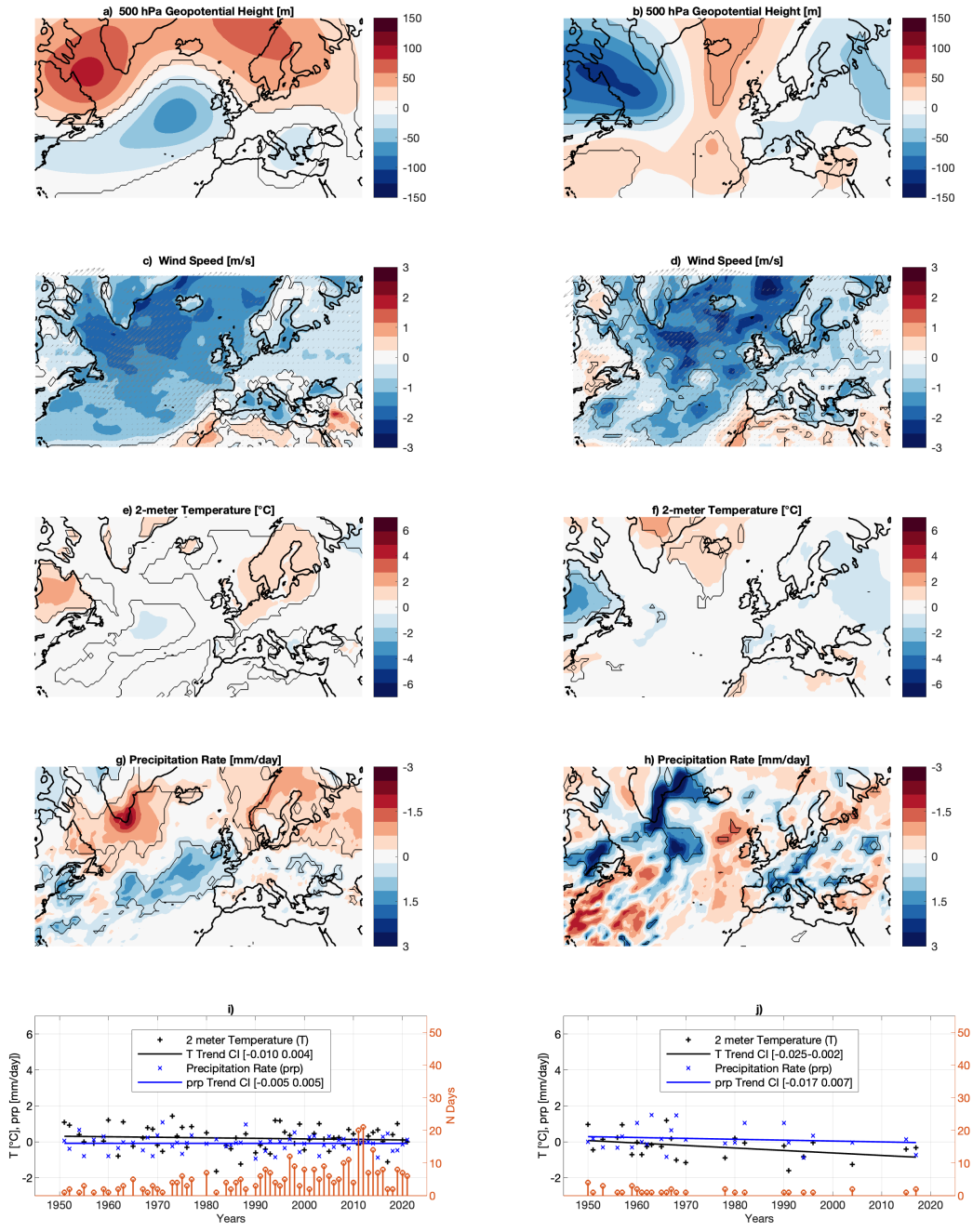

Figure S11. 500 hPa geopotential height summertime atmospheric circulation patterns with significant occurrence trends and associated surface anomalies: As in Fig. 2, but for 500 hPa geopotential height for ERA5 data (a,b).

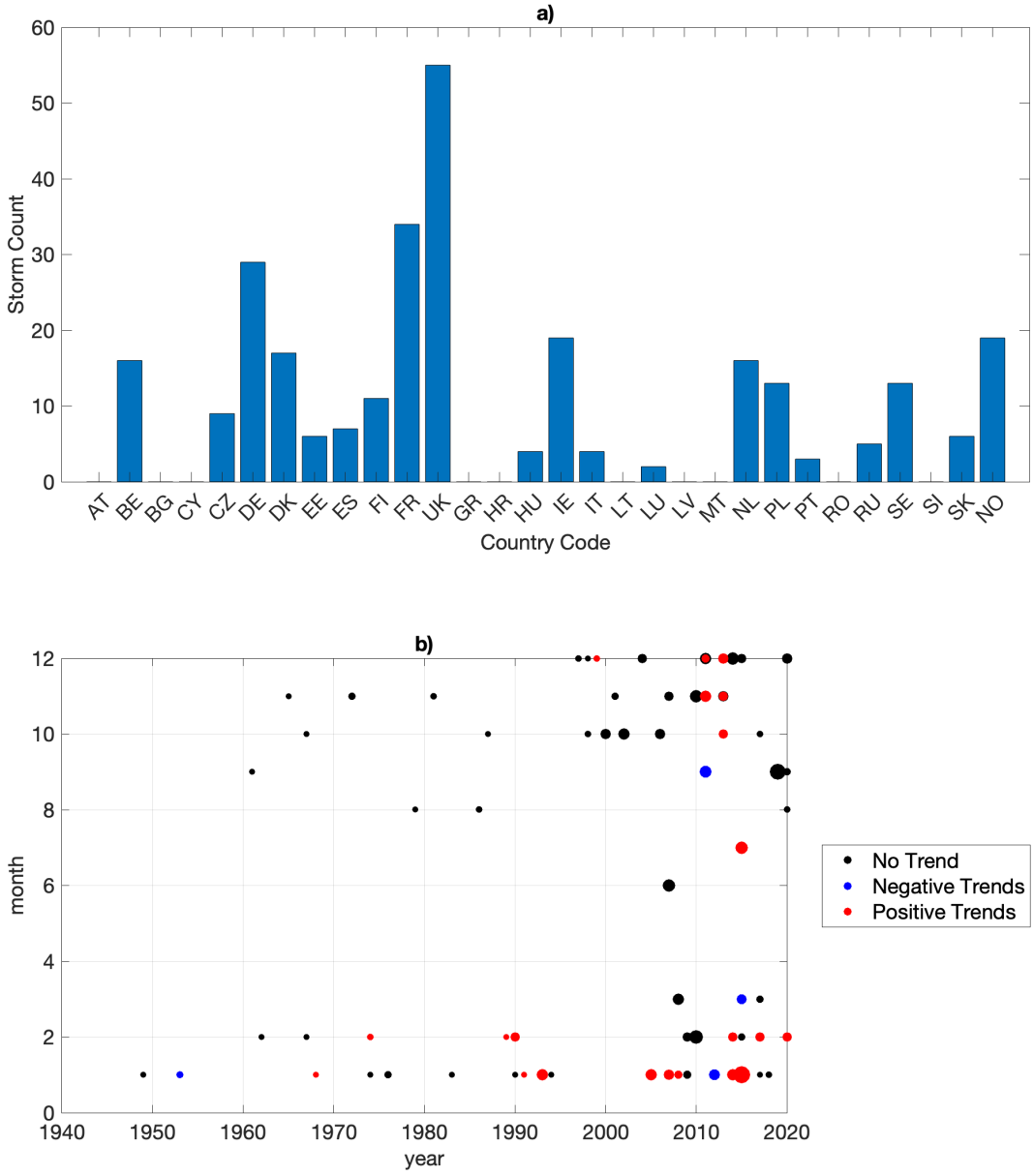

Figure S12. Spatial and temporal distribution of European windstorms: Number of European Windstorms per country (a). Year, month of occurrence of each storm and duration (size of the balls) and whether the storms are associated with atmospheric patterns displaying no (black), negative (blue) or positive (red) occurrence trends.

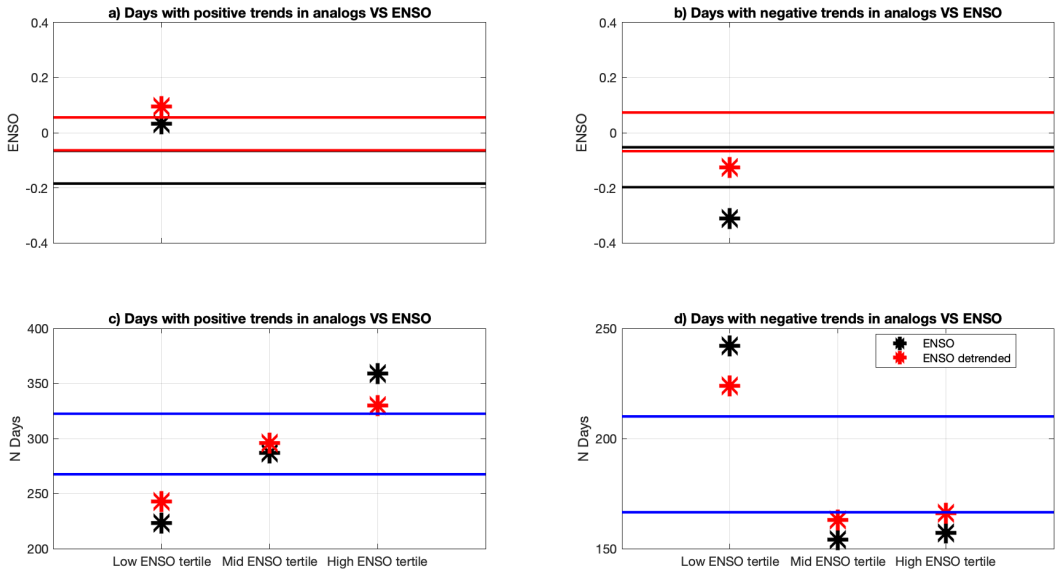

Figure S13. Monthly El Nino values conditioned on days with significant occurrence trends and count of days with significant occurrence trends corresponding to different El Nino phases: Averages of monthly El Nino 3.4 values conditioned on positive (a) or negative (b) occurrence trends (stars). Number of days with positive (c) or negative (d) occurrence trends during months with El Nino 3.4 values in the upper (right), middle (center) and lower (left) tertiles of the El Nino 3.4 index distribution. Results for both the raw and the linearly detrended El Nino timeseries are shown. The continuous lines correspond to the 5% significance bounds obtained by a bootstrapping procedure with 500 iterations.